Appl. Phys. B 75, 97–102 (2002)
DOI: 10.1007/s00340-002-0946-0

Applied Physics B
Lasers and Optics

W.G. BESSLER[1]
C. SCHULZ[1,✉]
T. LEE[2]
D.-I. SHIN[2]
M. HOFMANN[2]
J.B. JEFFRIES[2]
J. WOLFRUM[1]
R.K. HANSON[2]

Quantitative NO-LIF imaging in high-pressure flames

[1] Physikalisch-Chemisches Institut, Universität Heidelberg, 69120 Heidelberg, Germany
[2] Mechanical Engineering Department, Stanford University, Stanford, CA 94305, USA

Received: 13 May 2002
Published online: 8 August 2002 •

ABSTRACT Planar laser-induced fluorescence (PLIF) images of NO concentration are reported in premixed laminar flames from 1–60 bar exciting the $A - X(0, 0)$ band. The influence of O_2 interference and gas composition, the variation with local temperature, and the effect of laser and signal attenuation by UV light absorption are investigated. Despite choosing a NO excitation and detection scheme with minimum O_2-LIF contribution, this interference produces errors of up to 25% in a slightly lean 60 bar flame. The overall dependence of the inferred NO number density with temperature in the relevant (1200–2500 K) range is low ($< \pm 15\%$) because different effects cancel. The attenuation of laser and signal light by combustion products CO_2 and H_2O is frequently neglected, yet such absorption yields errors of up to 40% in our experiment despite the small scale (8 mm flame diameter). Understanding the dynamic range for each of these corrections provides guidance to minimize errors in single shot imaging experiments at high pressure.

PACS 42.62.Fi, 07.20.Dt, 42.62.Cf

1 Introduction

Quantitative imaging of nitric oxide concentrations with laser-induced fluorescence has attracted significant interest in recent years [1]. Measurements have been made in stable laminar flames [2] to develop and validate combustion models [3], and in practical applications [4] where simplified models describe combustion chemistry and transport in turbulent environments. Quantitative imaging measurements are also of interest to optimize combustor energy efficiency and minimize pollutant emission [5]. Although quantitative NO concentration imaging at high pressures has been made in internal combustion engines, to our knowledge no quantitative NO imaging measurements from laminar flames at elevated pressures have been published, although point measurements have been reported at 9 bar [6] and 15 bar [2].

At high pressures, selective detection of NO is crucial. O_2-LIF is an important source of interference for NO-LIF in high-pressure high-temperature fuel-lean environments [7]. The quantitative interpretation of NO-LIF is influenced by temperature in many respects, since not only ground state population distribution, but also line shapes and fluorescence-quenching cross-sections are temperature-dependent. The quenching rates depend upon local gas composition, which also varies with temperature. In the ultraviolet wavelength range below 250 nm used for NO diagnostics, strong absorption of laser and signal light by combustion products such as H_2O and CO_2 must be considered [8, 26], and this absorption strongly depends upon temperature. Finally, reliable calibration techniques are required [2, 9].

In steady laminar flames, these potential errors can be accounted for by sequentially measuring the temperature and modeling the concentration distributions of major species. This approach, however, is not possible for the investigation of turbulent flames commonly found in practical combustors. We assess here the relative importance of the different corrections in well-understood flames in order to determine the error margins introduced when these corrections are not quantitatively known. Therefore, we measure NO-LIF and background intensities in steady, laminar methane/air flames at 1–60 bar. Two-dimensional temperature distributions to correct for the various temperature-dependencies are obtained from multiple-line NO-LIF rotational thermometry [6].

2 Background

In systems with weak perturbation, the total signal for NO-LIF I_{LIF} is described according to (1) [10]:

$$I_{\mathrm{LIF}} \propto I_{\mathrm{laser}} T_{\mathrm{trans}}(p, T, x_i) \left(N_{\mathrm{NO}} f_{\mathrm{B}}(T) B g_{\lambda}(p, T) \phi(p, T, x_i) + S_{\mathrm{background}}(p, T, x_i) \right) . \quad (1)$$

In this regime the detected signal depends linearly upon the laser intensity I_{laser}. The overall transmission T_{trans} reflects the effects of laser and signal attenuation. The number of NO molecules in the laser-coupled quantum state is given by the number density N_{NO} times the Boltzmann coefficient f_{B}. The probability of their excitation depends on the incoming laser intensity, the Einstein B coefficient and the spectral overlap g_{λ} between the laser-spectral profile and absorption spectrum. These quantities depend strongly upon pressure p, local temperature T and species concentrations x_i. The ratio of excited

✉ Fax: +49-6221/545050,
E-mail: Christof.Schulz@pci.uni-heidelberg.de

molecules that are fluorescing is determined by the fluorescence quantum yield ϕ given in (2):

$$\phi = A/\left(A + Q(p, T, x_i) + P\right) . \quad (2)$$

For NO $A - X(0, 0)$ excitation at pressures above 1 bar, the denominator in (2) is dominated by Q. Therefore, ϕ_{NO} decreases strongly with pressure. O_2-LIF, in contrast, is strongly influenced by predissociation P when excited at the wavelengths considered here. Therefore, ϕ_{O_2} has a much reduced pressure-dependence. In practical systems, additional fluorescence background $S_{background}$ from interfering species, which also depends upon the laser intensity, is frequently present.

Equations (1) and (2) illustrate the five issues for quantitative NO-LIF in high-pressure flames.

(1) O_2-LIF interference: the transitions for hot-band O_2-LIF in the $B - X$ band overlap with the $A - X$ transitions of NO. Pressure broadening increases this overlap, and the relative O_2-to-NO quantum yield. The different pressure-dependence of the fluorescence quantum yield also decreases the NO-LIF/O_2-LIF ratio with increasing pressure. At high pressures it is therefore important to aim at maximum selectivity with the appropriate choice of excitation wavelength and detection filters. Recent work compared different alternatives for measuring NO-LIF in the $A - X(0, 0)$ band to minimize O_2 interference [11], and identified the preferable excitation scheme in a spectral region that has been previously used for flame studies [7, 12, 13]. Nevertheless, since the spectral overlap increases with pressure, a background signal $S_{background}$, which depends upon temperature, pressure and species concentrations contributes to the overall signal I_{LIF}. Ideally, this background should be measured independently either by tuning the laser off resonance [14, 15], or by calculating the contribution within the NO detection bandpass from measurements in other spectral regions [7]. In turbulent flames, however, the determination of this background is difficult. Therefore it is important to know the magnitude of the resulting errors from such interference when the background cannot be separately determined.

(2) Temperature dependence: Equation (1) contains several temperature-dependent factors. Not only is the population of the laser-coupled ground state temperature-dependent through the Boltzmann function f_B, but via the overlap g_λ. Furthermore, the quenching cross-sections and the frequency of collisions depend upon T, which yield a fluorescence quenching rate Q and, hence, for NO, a fluorescence quantum yield ϕ that varies with temperature. The corrections we apply are based on a spectral simulation code that includes line-broadening and shifting models [16–19]. NO transition frequencies and rotational line strengths (yielding the Einstein A and B coefficients) are calculated using relations from Paul [20], with vibrational transition probabilities taken from Laux and Kruger [21]. Figure 1 summarizes these temperature-dependent effects for the 1–60 bar pressure range. Temperature measurements in practical systems have been carried out simultaneously with NO-LIF measurements in a few cases [22], but generally such strategies are not feasible with the required accuracy. Therefore, temperature-insensitive techniques are advantageous in practical applications.

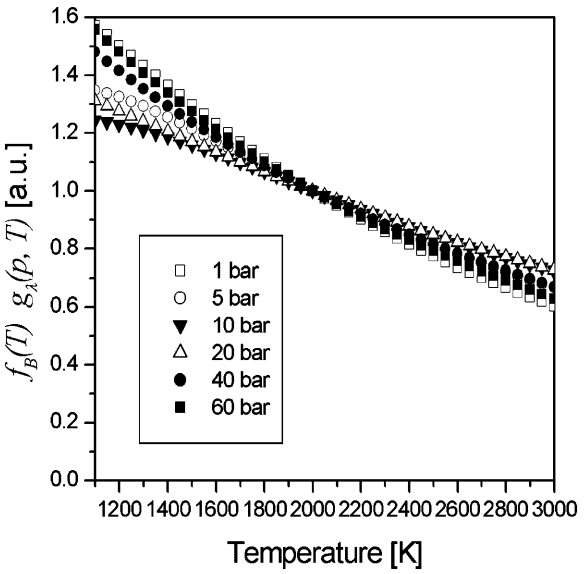

FIGURE 1 Simulated temperature-dependence of the NO-LIF excitation efficiency for the $A - X(0, 0)$ transition used in this work. The calculation includes the variation of the population of the laser-coupled level in the ground state and the overlap function g_λ, normalized at 2000 K

(3) Collisional quenching scales linearly with pressure when the gas composition is unchanged; however, the gas composition and the quenching cross-sections [23] are temperature-dependent. For the premixed flames here, chemical equilibrium can be assumed for measurements in the burnt gases. In homogeneously mixed systems where air/fuel ratios are invariant, the local quenching correction is a function of temperature only (Fig. 2). The influence of local variations in air/fuel ratios observed in direct injection engines has been discussed previously [24].

(4) Signal and laser absorption: recent experiments showed that in high-pressure high-temperature combustion environments, the UV transmission is reduced by absorp-

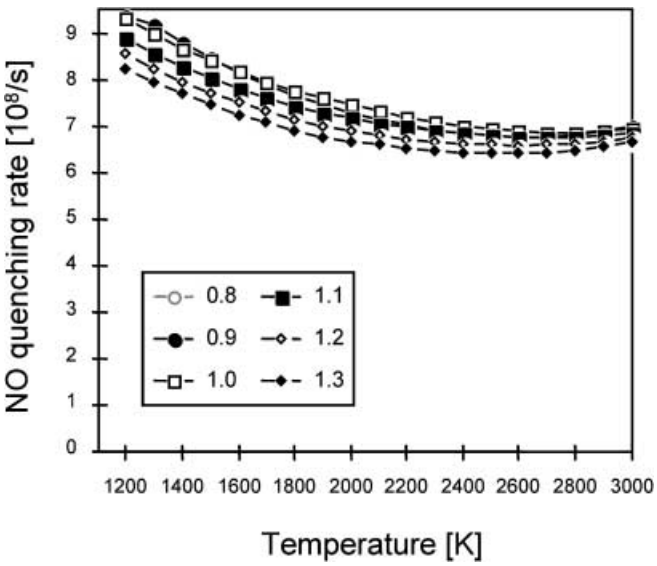

FIGURE 2 Temperature-dependence of the NO-LIF quenching rates in equilibrium burnt gases at fuel/air ratios from 0.8–1.3 at 10 bar (methane/air flame). Temperature-dependent quenching cross-sections are taken from [23]

tion by majority species like CO_2 and H_2O [25]. This attenuates both the laser and emitted fluorescence intensities (described by T_{trans} in (1)). Absorption cross-sections were recently determined in shock-tube experiments [8], and have been parameterized to facilitate practical applications [26]. Equilibrium concentrations of CO_2 in the burnt gas of stoichiometric 20 bar and 40 bar flames at 2200 K provide the same laser attenuation as 6500 ppm and 10 500 ppm NO, respectively, for a laser tuned on the strong NO absorption line used here. Thus, the CO_2 and H_2O absorption is much more important than NO-self absorption for reasonable NO concentrations. Note that pressure broadening decreases the effective absorption by NO. Therefore, laser attenuation by NO itself is negligible in our flames. The distributions of H_2O and CO_2 are well known in the burnt gas of a laminar flame with cylindrical geometry. Therefore, in this flame with equilibrium burnt gas composition, the resulting correction factors depend only upon the temperature distribution, and using a measured temperature, the magnitude of this correction is assessed below. Quantifying absorption in a turbulent flame is difficult; therefore these laminar flame determinations provide an upper bound for the potential error from hot combustion product absorption.

(5) Calibration: after corrections for all the above-mentioned effects, the NO-LIF signal is proportional to relative concentration throughout the observed area, and calibration is necessary to determine absolute concentration. The information required for calibration is determined here from NO-LIF in a series of flames with increasing NO seeding [4, 5, 14, 27]. NO addition in the 300–600 ppm range has a negligible influence on majority species concentrations and temperature. Larger and smaller concentrations of NO addition are perturbed by the prompt NO and NO reburn chemistries [28]. Using these seeding levels, NO destruction in slightly lean flames is expected to be below 10% [27], which is less than the errors resulting from NO-LIF calibration based on cell measurements at room temperature and atmospheric pressure [29]. Overall, NO-LIF is linearly proportional to NO seeding in slightly lean flames [9], and the in situ calibration measurement minimizes uncertainties due to variations in p, T, x_i. In our experiment, NO-addition measurements are carried out for each pressure independently. We compare the resulting calibration factors with the pressure dependence expected from spectral simulations, thus assessing the error introduced by calibration at a single fixed pressure for an experiment such as an IC engine with varying pressures.

3 Experimental

Laminar, premixed methane/air flat-flames at pressures from 1–60 bar were stabilized on a porous, sintered stainless steel plate of 8 mm in diameter. This burner was mounted in a stainless steel housing with an inner diameter of 60 mm with pressure stabilization ±0.1 bar [30]. Investigations were conducted for a $\phi = 0.95$ fuel/air equivalence ratio. An additional 2% (by volume) inert gas (NO/N_2 mixture with various NO concentrations) was added to the feedstock gases to allow NO seeding at the 0–600 ppm level without changing the dilution of the burnt gases. The total flow rates were adjusted for the various pressures in order to provide stable flat flames that allow the variation of air/fuel ratios, and these are listed in Table 1. The pressure variation of the flame temperature and natural NO concentration was not the aim of this study, and is not reported here.

Pressure [bar]	Measured NO mole fraction [ppm]	Measured NO number density [1/cm^3]	Total flow rate of fresh gases [ml/min]
1	23.8 ± 11%	$9.22 \times 10^{13} \pm 11\%$	750
5	27.7 ± 11%	$5.07 \times 10^{14} \pm 11\%$	1650
10	66.4 ± 11%	$2.45 \times 10^{15} \pm 11\%$	2250
20	137.2 ± 11%	$1.06 \times 10^{16} \pm 11\%$	3400
40	180.2 ± 12%	$2.62 \times 10^{16} \pm 11\%$	3810
60	141.8 ± 13%	$3.16 \times 10^{16} \pm 11\%$	4800

TABLE 1 Measured natural NO number densities and mole fractions in the central region 3 mm above the burner matrix. The right column gives the total flow rates of the premixed flame gases

Optical access to the flame was possible via four quartz windows (Fig. 3). Laser light (2 mJ @ 224–227 nm, 0.4 cm^{-1} FWHM) from a Nd:YAG-pumped (Quanta Ray GCR250) frequency-doubled (BBO) dye laser (LAS, LDL205) was formed into a vertical light sheet (5×0.5 mm^2) crossing the flame horizontally. It illuminates a cross-section through the center of the flame 1–6 mm above the burner matrix. The pulse energy was measured with a fast photodiode (LaVision). Fluorescence signals were collected at right angles to the laser beam and focused with a $f = 105$ mm, $f/4.5$ achromatic UV-lens (Nikon) onto the chip of an intensified CCD camera (LaVision FlameStar III). The signal light was discriminated against elastically scattered light with a 226-nm long-pass dielectric filter (Laser Optik), and an array of two high-reflection mirrors (HR @ 237 nm, FWHM 10 nm, Laser Optik).

The laser was tuned to the $P_1(23.5)$, $Q_1 + P_{21}(14.5)$, $Q_2 + R_{12}(20.5)$ absorption feature at 226.03 nm used in [7]. The background was measured off the NO resonance at 227.48 nm, which yields a comparable intensity of O_2-LIF. The images averaged over 50 laser shots were corrected for

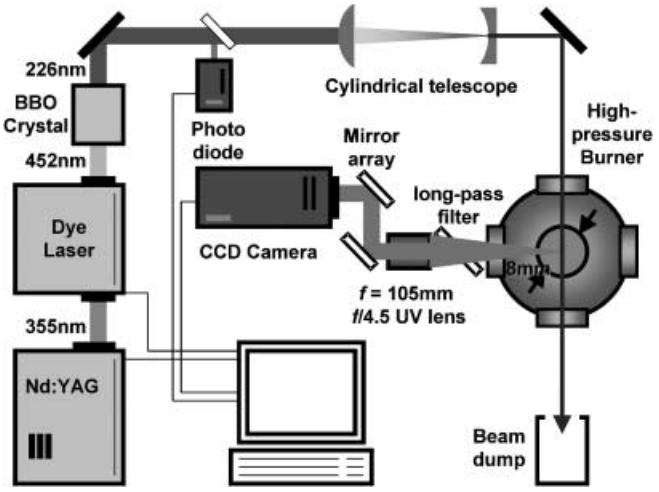

FIGURE 3 Experimental setup of the NO-LIF imaging experiment in the high-pressure burner

the light sheet intensity variations and spatial variations in detection efficiency.

The local temperature at each pixel is determined from a multi-point fit of the NO-LIF excitation spectra in the 225.95–226.10 nm range. This region corresponds to a broad minimum in O_2-LIF interference [7]. The laser is scanned (in 0.001 nm increments) and a stack of 2D images is obtained (with 300 ppm NO seed). The resulting 3D database (two spatial coordinates and the excitation wavelength coordinate) was then binned 3×3 on the spatial axis, and evaluated along the wavelength axis by a nonlinear least squares fit of the temperature-dependence of simulated LIF spectra. Thus, an approximate temperature field is obtained for the evaluation of quantitative NO-LIF images; however, a more complete investigation of the multiple-line temperature-imaging technique and a comparison with conventional two-line LIF-thermometry measurements is currently under way [31].

4 Results

NO is seeded into the feedstock of the premixed flame at concentrations in the 300–600 ppm range, yielding a linear increase in the signal. Figure 4 shows the calibration curves at different pressures. The measured signal intensities are corrected for attenuation and pressure- and temperature-dependence according to (1), and plotted versus seeded NO number densities. The calibration information that links measured pixel counts with local NO number densities is obtained only from the slopes. Varying offsets indicate different natural NO concentrations at the measurement location for the various flame conditions. The measurement position (3 mm above the burner matrix) is below the point of maximum NO concentration at 60 bar, which reduces the offset; conversely in the 40 bar flames this position is close to the maximum producing an increased offset. The second plot shows the slopes of the calibration curves with pressure. Because they are corrected for T- and p-effects, in the absence of measurement error, all the slopes should be identical. The variation ($\pm 10\%$) indicates the uncertainty from calibration at different pressures, errors in the spectra simulation, variation in NO reburn, and overall stability of the experiment.

The results of the imaging measurements are presented in Fig. 5 for six pressures in the $\phi = 0.95$ flame. Time-averaged, band-pass filtered, raw signals obtained with NO-excitation at 226.03 nm are shown in row (a). The measurements access the burnt gas region above the flat flame. Only the central cone of hot exhaust gases is stable; the outer part is increasingly unstable at high pressures and mixes with coflow air. Because the corrections are not all linear with temperature, significant systematic errors affect the signal interpretation in the fluctuating regions. We therefore use a statistical analysis of the signal standard deviation to constrain the quantitative investigation to the stable region, visible in row (b) as a green triangle.

Row (c) shows the off-resonant signal (227.48 nm excitation). Despite the use of the best possible excitation transition to discriminate against O_2-LIF [11], a contribution of background to the overall signal of 5, 9, 23 and 29% is present in the center of this slightly lean flame in the 1, 10, 40 and 60 bar flame, respectively. Images in rows (a) and (c) are not corrected for spatial variation in laser energy, and are presented with identical color scales.

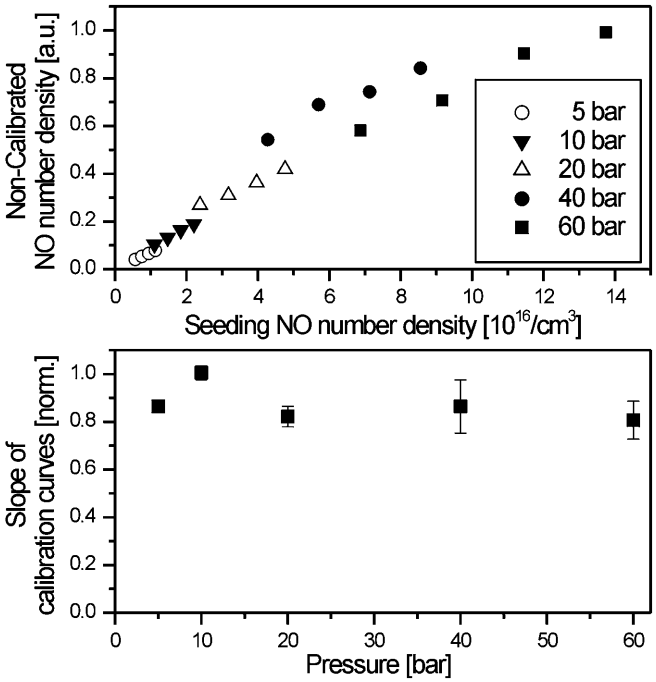

FIGURE 4 Calibration by NO seeding: The upper plot shows the linearity of the NO signal intensity versus NO seeding concentration at 5, 10, 20, 40 and 60 bar. The slopes of the resulting linear fits yield the calibration information and indicate the over-all NO-LIF yield. The lower plot compares these data with the results of spectra simulations taking into account all T and p-dependent terms of (1)

Row (d) displays temperature fields for the respective flames obtained from a multi-line fitting procedure. Measured temperatures in the central region for $\phi = 0.95$ are: 1870, 1981, 1968, 1862, 1967 K, at 1, 5, 10, 20 and 40 bar, respectively (all numbers refer to a measurement position 3 mm above the center of the burner head). For 60 bar, temperatures have not been measured by the multiple-line technique. For this condition we inferred the relative temperature from a two-line NO-LIF measurement calibrated to the multi-line temperature measurement at 40 bar. Calculations of adiabatic flame temperature show no significant variation in temperature in the 40–60 bar range. The temperature fields are used to calculate the corrections to the NO concentration from temperature-dependent variation of the NO spectra, Boltzmann fraction, the total number density, the quenching rate and T_{trans} the total transmission factor.

The dependence of the NO concentration measurement on local temperature variations is shown in rows (e) and (f). The NO concentration is computed for a temperature 200 K less than the measured temperature, and the ratio of the two computed concentrations $c_{\mathrm{NO}}(T - 200\,\mathrm{K})/c_{\mathrm{NO}}(T)$ is plotted in row (e) for number density and row (f) for mole fraction.

The temperature sensitivity is minimized for number density (row (e)), because the temperature-dependence of fluorescence quenching Q (Fig. 2) and the overall temperature-dependence of the ground state population and line broadening (Fig. 1) mostly cancel. Note the denominator of ϕ (2) for NO is dominated by Q; the two T-dependent correction factors shown in Figs. 1 and 2 are divided by each other in the cal-

culation of number density; thus, the temperature-dependent errors nearly cancel. Quenching depends linearly upon pressure, but in a complicated way on temperature through the change in the composition of the burnt gas. The equilibrium gas composition changes with T [32], whereas p only induces minor variations. Furthermore, T influences the quenching cross-sections and the individual collision frequencies. The resulting temperature-dependence of the quenching rate Q for different air/fuel ratios is shown in Fig. 2 for methane/air flames at 10 bar.

When NO mole fraction (row (f) in Fig. 5) is calculated instead of number density, an additional $1/T$ appears and the the T-sensitivity increases [33]. The images in row (f) indicate that in the central region a T-reduction by 200 K (for example, in a turbulent flow) would change the measurement by 6, 4, 2, 1.5, 4 and 5% at 1, 5, 10, 20, 40 and 60 bar. With increasing pressure the measurements become more robust due to the pressure broadened blur of the structure in the absorption spectrum. However, error in the NO mole fraction calculation from the 200 K T-uncertainty increases to a nearly constant 14% from the additional $1/T$ dependence. The overall temperature-sensitivity between 1200–2500 K increases from ±7%–18% (dependent on pressure) for measurements of NO number densities, and to ±38%–50% for measurements of NO mole fractions [33].

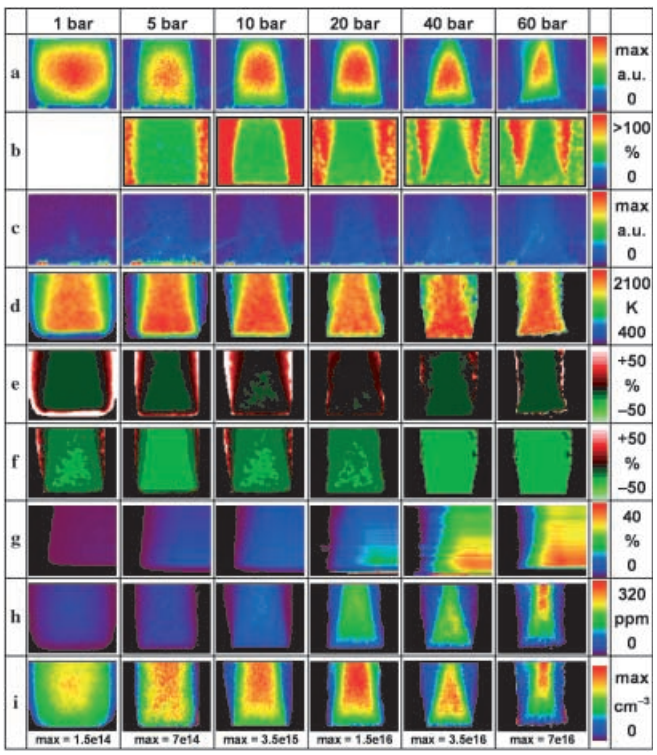

FIGURE 5 Results of the imaging analysis from the methane/air flame ($\phi = 0.95$, without NO seeding) at various pressures. **a** Raw NO-LIF images (not corrected for laser sheet inhomogeneities); **b** standard deviation derived from 250 instantaneous images (no data available at 1 bar); **c** raw off-resonant images (same color code as in **a**); **d** absolute temperatures from multi-line NO-LIF rotational thermometry measurements (for 60 bar: see text); **e** sensitivity of the NO number density on temperature variations of −200 K; **f** mole fraction measurements on temperature variations of −200 K; **g** total attenuation due to laser and signal absorption by CO_2 and H_2O; **h** quantitative NO mole fractions; **i** quantitative NO number densities

Row (g) displays the variation in transmission function T_{trans} including the effects of laser attenuation (at 226 nm) and signal attenuation (at 237 nm) based on CO_2 and H_2O absorption cross-sections, again using the temperature distribution and cylindrical symmetry of the flame. Despite the small size of the flame, total attenuation up to 43% is observed at 60 bar. The contribution of absorption by 100 ppm NO to the laser absorption caused by CO_2 and H_2O is 3.7, 2.2 and 1.0% at 1, 20 and 40 bar, respectively. Therefore, the hot CO_2 and H_2O are much more important absorbers than NO in most practical flames. To avoid interference by O_2-LIF the excitation wavelength for our LIF strategy is chosen to overlap with a pronounced minimum in the well-structured O_2 absorption spectrum. Thus, absorption by hot oxygen needs not to be taken into account.

The next two rows show the quantitative images of natural NO in the high-pressure flame as mole fractions (h) and number densities (i). These images are corrected for laser and signal attenuation and for all p- and T-dependent terms mentioned in (1). They are then calibrated using the measured calibration curves shown in Fig. 4. The resulting natural NO concentrations are listed in Table 1.

The overall accuracy for the quantitative measurements is ±11% for the NO number density measurements. The main contribution to the error is the systematic uncertainty of the calibration due to reburn of the seeded NO and overall experimental stability (estimated: ±10%, cf. Fig. 4). Errors in the measured temperature (resulting uncertainty on NO number density: ±1%–2%), the LIF measurement itself (ca. ±3%) and the spectral simulation code used for correcting the data (ca. ±2%), add up to 4%–5% (dependent on pressure). The overall accuracy decreases only slightly when determining NO mole fractions instead of number densities.

5 Conclusions

High-pressure LIF imaging measurements of NO number density and mole fraction have been carried out in $\phi = 0.95$ methane/air flames at 1–60 bar with an estimated accuracy of ±11% for the number density measurement. To our knowledge, these are the first quantitative PLIF images of NO at elevated pressure, and the first quantitative NO LIF measurements in well defined flames above 30 bar. NO concentrations are calibrated with NO seeded measurements. Temperatures are inferred from two-dimensional, multiple-line, rotational thermometry, and used to correct the signal intensities for temperature influence. The steady laminar flame allows a simple correction for non-resonant background contributions, primarily from LIF of hot molecular oxygen.

The impact of each correction is quantified to assess the error introduced in NO measurements in practical high-pressure combustors, where simultaneous measurements of temperature, background fluorescence and laser and signal attenuation are infeasible.

In the slightly lean flame, the background contribution that remains after tuning the laser off the NO resonance is nearly 25% (at 60 bar, relative to a natural NO concentration of 165 ppm), and is a significant contributor to the overall error when no corrections can be made. The total sensitivity of the NO number density measurements on temperature varia-

tions is surprisingly low because the effects of quenching (including the temperature-dependent variation of equilibrium burnt gas compositions) and the T-dependence of the spectra almost cancel in the 1200–2500 K range, and variations of ±7%–18% are observed over this temperature range [33]. However, mole fraction determination requires local temperature, and the resulting uncertainty when no information on local temperatures is available increases significantly. In applications with variable pressure (i.e. internal combustion engines), calibration is typically made at a single, fixed pressure. As long as the pressure-dependent effects are included in the data evaluation (rather then calibrating at each individual pressure), measurement uncertainties are not significantly increased.

Absorption by hot combustion products, CO_2 and H_2O, has often been ignored in previous work. Despite the small size of our flame (8 mm diameter), the total attenuation of laser excitation and signal light at 60 bar is nearly 45%. Thus, absorption is of major concern for quantitative NO measurement, especially in larger scale practical applications.

ACKNOWLEDGEMENTS Work at Stanford supported by the US Air Force Office of Scientific Research, Aerospace Sciences Directorate, with Julian Tishkoff as the technical monitor. The Division of International Programs at the US National Science Foundation supports the Stanford collaboration via a cooperative research grant. The University of Heidelberg work and the travel of WB and CS are sponsored by the Deutsche Forschungsgemeinschaft (DFG) and the Deutsche Akademische Auslandsdienst (DAAD).

REFERENCES

1 J. Wolfrum: Proc. Combust. Inst. **27**, 1 (1998)
2 J.R. Reisel, N.M. Laurendeau: Combust. Sci. Technol. **98**, 137 (1994)
3 R.V. Ravikrishna, N.M. Laurendeau: Combust. Flame **120**, 372 (2000)
4 G. Josefsson, I. Magnusson, F. Hildenbrand, C. Schulz, V. Sick: Proc. Combust. Inst. **27**, 2085 (1998)
5 W.G. Bessler, C. Schulz, M. Hartmann, M. Schenk: SAE Technical Paper Series No. 2001-01-1978 (2001)
6 A.O. Vyrodow, J. Heinze, M. Dillmann, U.E. Meier, W. Stricker: Appl. Phys. B **61**, 409 (1995)
7 M.D. DiRosa, K.G. Klavuhn, R.K. Hanson: Combust. Sci. Technol. **118**, 257 (1996)
8 C. Schulz, J.D. Koch, D.F. Davidson, J.B. Jeffries, R.K. Hanson: Chem. Phys. Lett. **355**, 82 (2002)
9 C. Schulz, V. Sick, U. Meier, J. Heinze, W. Stricker: Appl. Opt. **38**, 1434 (1999)
10 A.C. Eckbreth: *Laser Diagnostics for Combustion Temperature and Species*, 2nd Ed. (Gordon & Breach 1996)
11 W.G. Bessler, C. Schulz, T. Lee, D.-I. Shin, J.B. Jeffries, R.K. Hanson: Appl. Opt. (2002) in press
12 B.E. Battles, R.K. Hanson: J. Quant. Spectrosc. Radiat. Transfer **54**, 521 (1995)
13 J.E. Dec, R.E. Canaan: SAE Technical Paper Series No. 980147 (1998)
14 D.D. Thomsen, F.F. Kuligowski, N.M. Laurendeau: Appl. Opt. **36**, 3244 (1997)
15 F. Hildenbrand, C. Schulz, J. Wolfrum, F. Keller, E. Wagner: Proc. Combust. Inst. **28**, 1137 (2000)
16 A.Y. Chang, M.D. DiRosa, R.K. Hanson: J. Quant. Spectrosc. Radiat. Transfer **47**, 375 (1992)
17 M.D. DiRosa, R.K. Hanson: J. Mol. Spectrosc. **164**, 97 (1994)
18 M.D. DiRosa, R.K. Hanson: J. Quant. Spectrosc. Radiat. Transfer **52**, 515 (1994)
19 A.O. Vyrodov, J. Heinze, U.E. Meier: J. Quant. Spectrosc. Radiat. Transfer **53**, 277 (1995)
20 P.H. Paul: J. Quant. Spectrosc. Radiat. Tranfer **57**, 581 (1997)
21 C.O. Laux, C.H. Kruger: J. Quant. Spectrosc. Radiat. Tranfer **48**, 9 (1992)
22 C. Schulz, V. Sick, J. Wolfrum, V. Drewes, M. Zahn, R. Maly: Proc. Combust. Inst. **26**, 2597 (1996)
23 P.H. Paul, J.A. Gray, J.L. Durant Jr., J.W. Thoman Jr.: Appl. Phys. B **57**, 249 (1993)
24 F. Hildenbrand, C. Schulz, M. Hartmann, F. Puchner, G. Wawrschin: SAE Technical Paper Series No. 1999-01-3545 (1999)
25 F. Hildenbrand, C. Schulz: Appl. Phys. B **73**, 173 (2001)
26 C. Schulz, J.B. Jeffries, D.F. Davidson, J.D. Koch, J. Wolfrum, R.K. Hanson: Proc. Combust. Inst. 29 (2002) in press
27 A.V. Mokhov, H.B. Levinsky, C.E. van der Meij: Appl. Opt. **36**, 3233 (1997)
28 J. Warnatz, U. Maas, R.W. Dibble: *Combustion* (Springer, Heidelberg 1996)
29 P.A. Berg, G.P. Smith, J.B. Jeffries, D.R. Crosley: Proc. Combust. Inst. **27**, 1377 (1998)
30 H. Eberius, T. Just, T. Kick, G. Höfner, W. Lutz: Proc. Joint Meeting German/Italian Section Comb. Inst., Ravello, Italy, 3.3 (1989)
31 W.G. Bessler, C. Schulz, T. Lee, J.B. Jeffries, R.K. Hanson: Appl. Opt. In preparation (2002)
32 D. Schmidt: *Methane/air equilibrium calculations*, ITV, University of Stuttgart (1998)
33 W.G. Bessler, C. Schulz, D.-I. Shin, T. Lee, J.B. Jeffries, R.K. Hanson: Laser Applications to Chemical and Environmental Analysis. In: OSA Topical Meeting (2002)